Dalton Transactions

ROYAL SOCIETY OF CHEMISTRY

PAPER

View Article Online
View Journal | View Issue

Cite this: *Dalton Trans.*, 2023, **52**, 3158

Dual visible and near-infrared luminescence in mononuclear macrocyclic erbium(III) complexes *via* ligand and metal centred excitation†

Yolimar Gil, *[a] Ricardo Costa de Santana, *[b] Andréa Simone Stucchi de Camargo, [c] Leonnam Gotardo Merízio, [c] Patricia Farías Carreño, [a] Pablo Fuentealba, [a] Jorge Manzur[a] and Evgenia Spodine [a]

Received 24th October 2022,
Accepted 7th February 2023

DOI: 10.1039/d2dt03447f

rsc.li/dalton

Considering the structural design of some of the scarce molecular-based Er-centred emitters in the literature, we explored the optical properties of three Er^{III} hexaazamacrocyclic complexes, namely Er-EDA (**1**), Er-OPDA(**2**) and Er-DAP(**3**). The macrocyclic ligands in these complexes differ in the lateral spacers, and are derived from 2,6-pyridine-dicarbaldehyde and ethylenediamine (EDA), *ortho*-phenylenediamine (OPDA) or 1,3-diaminopropane (DAP). Upon ligand-centred excitation, the bluish-green and green emissions of the Er^{III} ion were detected only for the complexes containing macrocycles with aliphatic spacers (**1** and **3**), which evidenced that these ligands can sensitize the Er^{III} luminescence. On the other hand, the ligand derived from the aromatic diamine (**2**) does not sensitize the Er^{III} luminescence. Energy transfer mechanisms, temperature sensing, CIE coordinates and CCT values were analyzed. Besides the excitation in the ligands, the erbium-centred excitation at 980 nm allowed the detection, in all cases, of bluish-green, green and red up-converted emissions, and also the downshifted NIR emission. The possible mechanisms involved in these transitions were described and analyzed according to the available data.

Introduction

Trivalent lanthanide ions have been widely studied due to their exceptional luminescence features such as narrow bandwidths, long-lived emission, and large Stokes shifts.[1] Among the lanthanides, Er^{III} ions ($4f^{11}$ configuration) exhibit some regularly spaced distribution of $^{2S+1}L_J$ excited levels, giving rise to bluish-green ($^2H_{11/2} \rightarrow {}^4I_{15/2}$), green ($^4S_{3/2} \rightarrow {}^4I_{15/2}$), red ($^4F_{9/2} \rightarrow {}^4I_{15/2}$), and near-infrared ($^4I_{13/2} \rightarrow {}^4I_{15/2}$) emission bands, which make them suitable for a wide variety of applications such as bioprobes and sensors in living organisms.[2–4] These regularly spaced excited states are a requirement for linear energy down-conversion (DC) and non-linear up-conversion (UC).[5] The first term consists of the conversion of one photon of high energy into two photons of lower energies, while UC implies the sequential absorption of two or more low-energy photons to produce the emission of a photon of higher energy.[6,7] These optical processes depend on the existence of long-lived intermediate excited states, being pivotal that non-radiative relaxation processes are prevented.[8] In this sense, up-conversion has been mainly investigated in low-phonon inorganic solids or nanoparticles doped with Er^{III} ions for a range of applications including bioimaging.[9–11] Additional drawbacks of inorganic nanomaterials are related to the synthetic reproducibility and potential toxicity due to their inability to be removed from the body post-imaging, which prevents their potential clinical application.[12] In this sense, the design of erbium coordination complexes with improved excited-state lifetimes seems to be a favourable alternative to bring these materials to biomedical applications. The strategy in the design of these complexes is to achieve a low-energy phonon environment being necessary to avoid high-energy C–H, C–O, N–H and O–H stretching vibrations close to the metal centre, which are known as efficient luminescent quenchers.[13] The solvent also plays an important role in the quenching phenomena;[14] therefore it is important to prevent the coordination of solvent molecules or second sphere interactions with

[a]*Facultad de Ciencias Químicas y Farmacéuticas, Universidad de Chile, Olivos 1007, 8380544 Santiago, Chile. E-mail: gil.yolimar@gmail.com, jmanzursaf@gmail.com, espodine@uchile.cl, pfuentealbacastro@ciq.uchile.cl, pcfariasc@gmail.com*

[b]*Instituto de Física, Universidade Federal de Goiás, Campus Samambaia, 74690-900 Goiânia, GO, Brazil. E-mail: santana@ufg.br*

[c]*Instituto de Física de São Carlos, Universidade de São Paulo, Avenida Trabalhador São-Carlense, nº400 Parque Arnold Schimidt, CEP, 13566-590 São Carlos, SP, Brazil. E-mail: lmerizio@ifsc.usp.br, andreasc@ifsc.usp.br*

†Electronic supplementary information (ESI) available: Diffuse reflectance, NIR emission, phosphorescence and up-conversion and downshifting spectra of the complexes. See DOI: https://doi.org/10.1039/d2dt03447f

the erbium(III) ion. Considering the high coordination number of trivalent erbium which is around 8–9, preorganized multidentate ligands have been used to shield the lanthanide centre from interactions with high-energy oscillators of ligands or solvent molecules.[5,15] In recent years, this strategy has been implemented by building highly protected triple helical erbium complexes possessing nine-coordinate $[ErN_3O_6]$ and $[ErN_9]$ chromophores.[15–18] These complexes exhibit dual downshifted NIR and visible (green) emission bands under ligand excitation and metal-centred excitation. In the case of complexes with an $[ErN_9]$ coordination geometry, the erbium(III) ion is coordinated by nine neutral heterocyclic nitrogen donor atoms, which are known to provide a weak crystal field. This type of crystal field in erbium complexes leads to a minimum splitting of J manifolds, minimizing multi-phonon non-radiative relaxations and consequently improving the up-conversion efficiency.[5]

Taking into account these strategies, hexaazamacrocyclic ligands derived from 2,6-pyridine-dicarbaldehyde and diamines such as ethylenediamine (EDA), *o*-phenylenediamine (OPDA), and 1,3-diaminepropane (DAP) (Fig. 1), can potentially fulfil the requirements to improve the up-conversion in mononuclear Er^{III} complexes. These macrocycles guarantee an hexacoordination around the erbium ion which protects from second sphere interactions. On the other hand, the six neutral nitrogen donor atoms in the macrocycle produce the required weak crystal field.

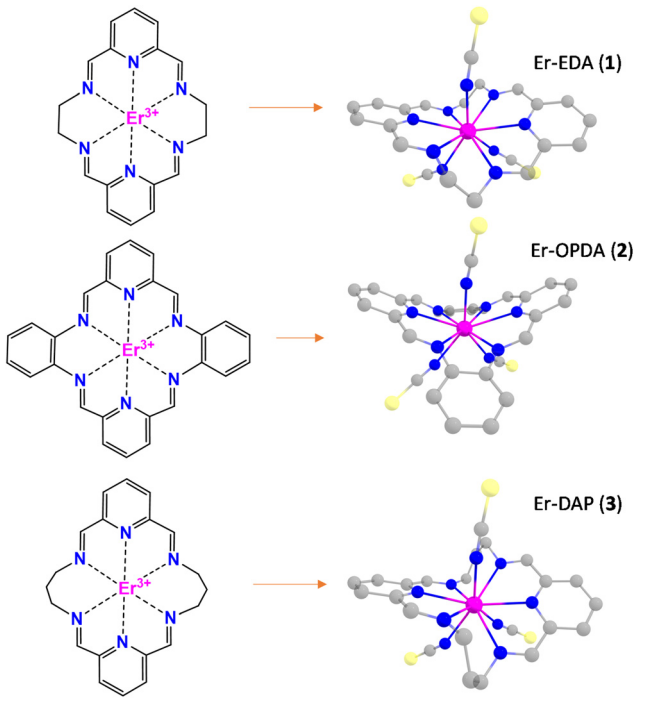

Fig. 1 Scheme of the hexaazamacrocyclic ligands in complexes **1–3** (left) and molecular structures of the corresponding Er^{III} complexes, where the $[ErN_9]$ coordination sphere is highlighted in solid colors (right). Color code: Er (pink), N (blue), C (grey), and S (yellow).

In this sense, we evaluated the luminescence of three hexaazamacrocyclic Er^{III} complexes with isothiocyanate ligands and possessing an $[ErN_9]$ coordination geometry (Fig. 1). Macrocyclic ligands with aliphatic spacers were shown to act as antennas to sensitize the erbium(III) luminescence, and, as we expected, up-conversion and downshifting were also detected upon metal-centred excitation. Interestingly, these macrocyclic complexes exhibited an up-converted red emission, which, to our knowledge, is unprecedented in solid-state mononuclear Er^{III} complexes.

Experimental

Synthesis

Reagent grade chemicals and HPLC quality solvents were used as received. The synthesis of erbium(III) complexes **1–3** was performed according to the reported procedures[19,20] (see the ESI†).

Physical measurements

Diffuse reflectance spectra were recorded using a PerkinElmer Lambda WB1050 spectrophotometer. All optical measurements were performed using finely ground powder samples. PL emission spectra were recorded using a Horiba-Jobin Yvon spectrofluorimeter, model Fluorolog-3 (FL3-221), under excitation with a 450 W Xe lamp and detection using a Horiba PPD-850 picosecond photon detector for the UV-VIS region, and an InGaAs detector for the IR region. In the excitation and emission experiments, the slits used were 5 nm for the UV-VIS region and 4 nm for the IR region. The PL emission spectra were corrected for the spectral response of monochromators and the detector using the standard correction file provided by the manufacturer. Up-conversion experiments were carried out using a Horiba-Jobin Yvon fluorimeter, model Fluorolog-3 FL-1050, equipped with a PPD-850 detector and an OptoEngine LLC model MDL-III 980 2W detector, and an adjustable laser diode (980 nm) as the excitation source. Phosphorescence experiments on Y^{III} complexes were performed at 20 K and with delays varying from 0.005 to 0.05 ms using a Xe pulsed lamp, slits of 7 nm, and the same setup described for luminescence experiments. For NIR and up-conversion photoluminescence experiments with diode lasers (Crystal Laser LC), a wavelength of 980 nm was used. Low-temperature experiments were performed using a closed cycle cryostat operating with a Lake Shore temperature controller.

The thermometric parameter Δ for both intensity ratios, $I_{^4S_{3/2}}/I_{ligand}$ and $I_{^4S_{3/2}}/I_{^2H_{11/2}}$, was obtained from eqn (1):[21]

$$\Delta = \Delta_0/(1 + C\exp(-\Delta E_A/kT)) \quad (1)$$

while the $I_{^4S_{3/2}}/I_{ligand}$ ratio for **1** was obtained from eqn (2):[21]

$$\Delta = \Delta_0/(1 + C_1\exp(-\Delta E_{A1}/kT) + C_2\exp(-\Delta E_{A2}/kT)). \quad (2)$$

In both equations, Δ_0 is the thermometric parameter at T = 0 K, C is the ratio between the non-radiative and radiative probabilities, and ΔE_A is the activation energy for the non-

radiative channel. The relative sensitivities, S_r, for **1** and **3** were calculated using eqn (3):

$$S_r = 100\%|(\partial\Delta/\partial T)/\Delta| \quad (3)$$

where $\partial\Delta$ is the variation of the thermometric parameter for a certain temperature variation (∂T).

Results and discussion

Structural description

Fig. 1 shows the molecular structures of the hexaazamacrocyclic Er^{III} complexes. All complexes have a nine-coordinated Er^{III} centre, where the neutral macrocyclic ligand is coordinated through six nitrogen atoms, and outside of the macrocycle plane, three monodentate isothiocyanate anions complete the coordination sphere. These complexes differ in the lateral spacers in the macrocycle, which consists of an aromatic ring (OPDA) for complex **2**, and aliphatic chains of two and three carbon atoms for **1** (EDA) and **3** (DAP), respectively.[1]

Photoluminescence studies

Two excitation sources were used to obtain the photoluminescence of the studied erbium(III) species: a xenon lamp was used to excite at 370 nm, which generates photons that are solely absorbed by the organic ligands, and a 980 nm laser, which allows the absorption of energy by the erbium(III) ions.

Ligand sensitized photoluminescence

Fig. 2a shows the normalized solid-state excitation spectra of all the studied Er^{III} complexes recorded at room temperature obtained by monitoring the emission at 542 nm ($^4S_{3/2} \rightarrow {}^4I_{15/2}$ transition) for **1** and **3**, and at 472 nm for **2**. The spectra show broad bands in the range of 250–430 nm, corresponding to the $\pi \rightarrow \pi^*$ electronic transitions of the ligands. Above 430 nm, the excitation spectra of **1** and **3** show some peaks associated with Er^{III} 4f–4f electronic transitions from the ground level $^4I_{15/2}$ to the excited levels $^4F_{3/2}$ (444 nm), $F_{5/2}$ (450 nm), $^4F_{7/2}$ (487 nm) and $^2H_{11/2}$ (521 nm).[22] No evidence of f–f Er^{III} transitions was observed in the excitation spectrum of **2** under the measurement conditions.

As the 4f–4f transitions are forbidden by spin and parity (Laporte's rules), the Ln^{III} ions have very small molar absorption coefficients, which result in weak emissions.[22] To improve the Ln^{III} absorptions, the most commonly used mechanism, since Weissman pioneering work,[23] involves the use of organic ligands, which can act as chromophores and promote an efficient energy transfer to the emissive metal energy levels. This energy transfer produces a light-downshifting, the so-called "antenna effect".[3] Therefore, the sensitization of erbium(III) was mediated by the ligand centred excitation source. Fig. 2b shows the normalized emission spectra at room temperature of **1–3** in the UV-visible region (390 to 700 nm) under excitation of the ligands at 370 nm.

The emission spectra of **1** and **3** are similar, both exhibit broad bands with two maxima at 416 and 436 nm, which are attributed to intraligand transitions. At lower energies, two sharp peaks centred at 523 (bluish-green) and 542 nm (green) were detected, which are assigned to the $^2H_{11/2} \rightarrow {}^4I_{15/2}$ and $^4S_{3/2} \rightarrow {}^4I_{15/2}$ transitions of the Er^{III} ion, respectively.[22] In both cases, this last transition shows an absolute intensity higher than that of $^2H_{11/2} \rightarrow {}^4I_{15/2}$, which can be explained as follows. The excited states $^2H_{11/2}$ and $^4S_{3/2}$ are thermally coupled levels (TCL) for which the probability of transitions between them at temperature T follows the Boltzmann distribution law and can be expressed as follows:

$$\%(N_{bg}/N_g) = \exp(-\Delta E/KT) \times 100$$

where ΔE is the energy gap between both levels, K is the Boltzmann constant, and $N_{bg}$and N_g are the population of $^2H_{11/2}$ and $^4S_{3/2}$ excited states, respectively.[24] At room temperature the $\%(N_{bg}/N_g)$ value is low (3.6%). Therefore, the emission at 523 nm is less intense than that at 542 nm.

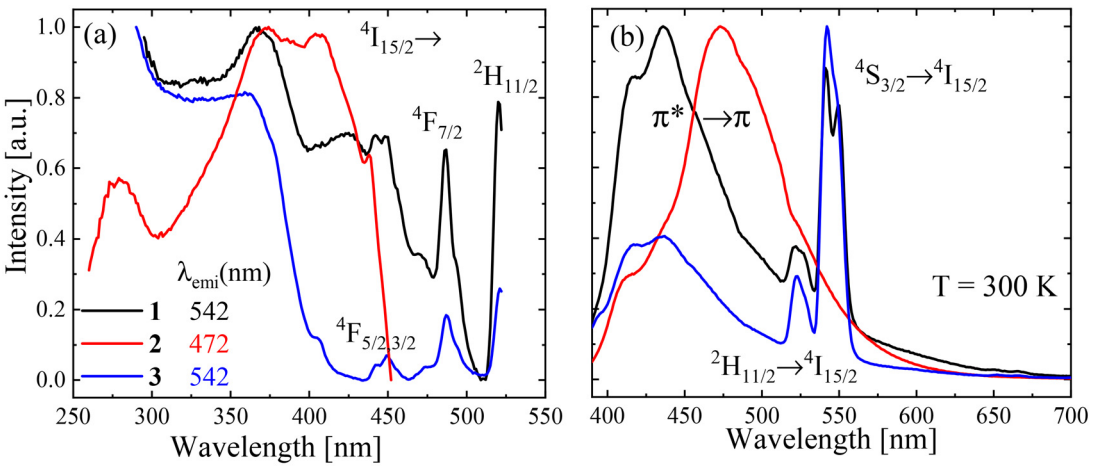

Fig. 2 Normalized solid state (a) excitation and (b) photoluminescence spectra at room temperature upon ligand-mediated excitation in the UV region (λ_{exc} = 370 nm) of **1–3**.

Comparing the absolute intensity of the green emission ($^4S_{3/2} \rightarrow {}^4I_{15/2}$) of the Er^{III} ion with that of the ligand band, it is possible to observe that for **1** both are of the same order of magnitude. However, for **3**, the $^4S_{3/2} \rightarrow {}^4I_{15/2}$ transition is of higher intensity than that of the ligand emission band. This is in agreement with the excitation spectra (Fig. 2a), where the ligand band is of higher intensity with respect to the f–f transitions in **3**, evidencing that the energy transfer from the ligand to the emissive state of Er^{III} is more efficient for **3** than for **1**. The emission spectrum of **2** shows a broad band centred at 474 nm, corresponding to an intraligand transition, and no clear evidence of the Er^{III} emission was observed. On the other hand, the characteristic erbium(III) emission band in the NIR region (*ca.*1500 nm) was detected for the studied hexaazamacrocyclic complexes **1** and **3** when the 370 nm excitation energy was used. However, this signal was extremely weak, as can be seen in Fig. S2.† In the case of **2**, this NIR emission was not detected. Thus, NIR emission at *ca.* 1500 nm, due to the antenna effect, is not an efficient process for the studied complexes.

Fig. 3 shows the proposed downshifting mechanism following ligand-centred excitation for **1** and **3**, which implies an energy transfer from the T_1 excited state of the macrocyclic ligand EDA or DAP (25 063 cm^{-1}) (see the ESI†) to the nearest excited state $^2G_{9/2}$ (24 400 cm^{-1})[25] of the Er^{III} ion. From this level, multiple non-radiative relaxations to the $^2H_{11/2}$ and $^4S_{3/2}$ excited states give rise to $^2H_{11/2} \rightarrow {}^4I_{15/2}$ and $^4S_{3/2} \rightarrow {}^4I_{15/2}$ transitions. Besides, multiple non-radiative relaxations occur from $^4S_{3/2}$ to $^4I_{13/2}$, with which an extremely weak near-infrared emission corresponding to the $^4I_{13/2} \rightarrow {}^4I_{15/2}$ transition is obtained. In the case of the OPDA ligand, the energy transfer from the T_1 excited state (20 618 cm^{-1}) to the excited states of the Er^{III} ion is not feasible, and no emission bands were detected for **2**.

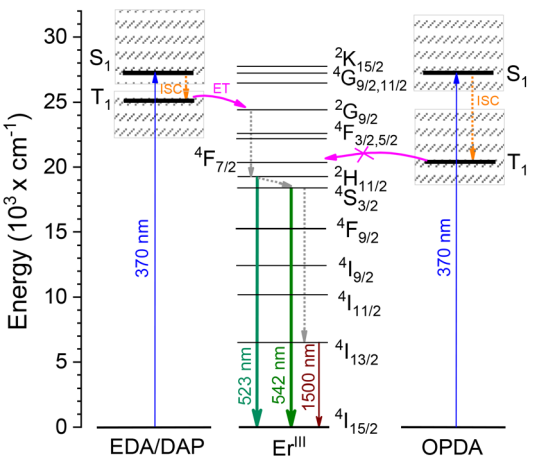

Fig. 3 Energy level diagram showing the downshifting process by ligand-centred excitation (blue upward arrows), intersystem crossing (ISC, orange dotted arrows), energy transfer (ET, pink curved arrows), non-radiative decay (grey dotted arrows), and radiative emission (solid downward arrows) for **1**, **2** and **3**, where the macrocyclic ligands are EDA, OPDA and DAP, respectively.

Temperature-dependent luminescence

The luminescence properties of **1** and **3** were investigated as a function of the temperature in the range of 17–300 K. The normalized solid-state emission spectra of these complexes under excitation at 370 nm are presented in Fig. 4a and b, respectively. No change in the position of the ligand or Er^{III} emissions was observed over the entire temperature range. A decrease in the emission intensities of Er^{III} bands with increasing temperature was observed that could be attributed to the non-radiative thermal deactivation.

Fig. 4c and d show the emission spectra of **1** and **3** at selected temperatures, respectively. In all spectra, bands due to the ligand and erbium cation were observed. The most intense ligand emission was detected for **1** that overlaps with the $^2H_{11/2} \rightarrow {}^4I_{15/2}$ and $^4S_{3/2} \rightarrow {}^4I_{15/2}$ transitions, and this overlap is stronger for the former. For **3** as the ligand emission is weaker, only the $^2H_{11/2} \rightarrow {}^4I_{15/2}$ transition is slightly overlapped. In order to evaluate the potential of **1** and **3** as luminescent thermometers, the thermal dependence of the ratio between the integrated areas of two emission bands was used, being in this study the $I_{^4S_{3/2}}/I_{ligand}$ and $I_{^4S_{3/2}}/I_{^2H_{11/2}}$ ratios. According to Cui *et al.*,[26] this type of dual luminescent thermometer avoids the influence of the excitation source and detector on the obtained values. Fig. 5a and b show the $I_{^4S_{3/2}}/I_{ligand}$ ratio and the insets show the relative sensitivities as a function of temperature for **1** and **3**, respectively. In both complexes, the $I_{^4S_{3/2}}/I_{ligand}$ ratio is lower than the unity in the entire temperature range (17–300 K), this due to the higher integrated area of the ligand band with respect to that of the $^4S_{3/2} \rightarrow {}^4I_{15/2}$ transition. For **1** an oscillant curve was obtained, while for **3** the ratio presents an almost constant value below 90 K and then decays linearly until 300 K, with this linear behaviour being useful for thermometry The maximum sensitivity for **3** was obtained at 190 K with a value of 0.16% K^{-1} (Table 1).

As was described above, the excited states $^2H_{11/2}$ and $^4S_{3/2}$ are thermally coupled levels, thus the transitions from these excited states to the $^4I_{15/2}$ ground state will exhibit a thermal dependence.[27,28] In this way, the ratio between the integrated areas of the $^2H_{11/2} \rightarrow {}^4I_{15/2}$ and $^4S_{3/2} \rightarrow {}^4I_{15/2}$ transitions ($I_{^4S_{3/2}}/I_{^2H_{11/2}}$) was also used for optical thermometric studies in the temperature range of 17–300 K (Fig. 5c and d). This ratio shows, in both cases, a similar behavior. For **1**, the ratio remains almost constant below 110 K and then decreases from 8.6 at 130 K to 4.0 at 300 K. On the other hand, for **3** the ratio value decreases slowly from 8.6 at 30 K to 7.9 at 130 K and then decreases linearly to 4.0 at 300 K. As observed in Fig. 5, the most pronounce decrease is observed for **1** that is the complex with a higher sensitivity of 0.58% K^{-1} at 270 K.

Table 1 summarizes the thermometric parameters, presenting the S_r value at room temperature and the maximum S_r value at a given temperature. The obtained S_r values reveal one advantage of these complexes, which is that two ratios can be used to evaluate the thermal sensitivity. For **1** the optimal S_r value was obtained using $I_{^4S_{3/2}}/I_{ligand}$ at room temperature, while **3** showed the maximum value for $I_{^4S_{3/2}}/I_{^2H_{11/2}}$ at 250 K (Table 1). Therefore, both complexes may be used as potential ratiometric sensors.

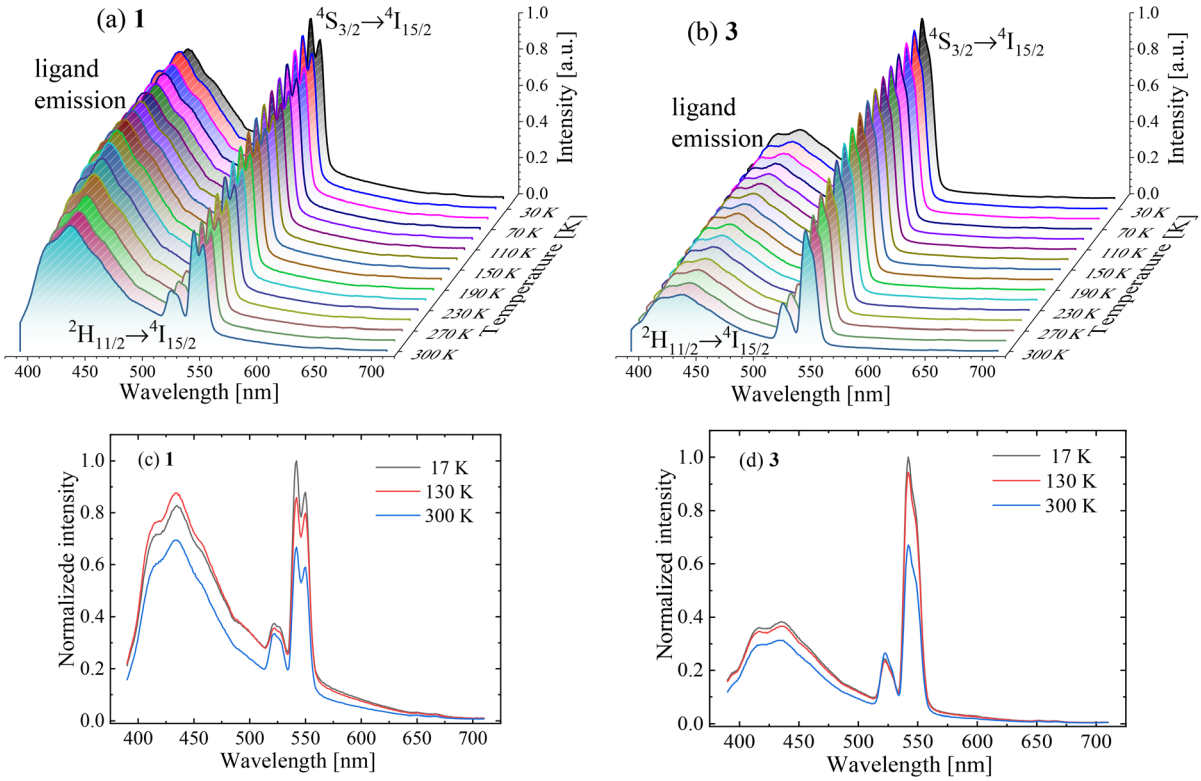

Fig. 4 Thermal dependence of the normalized solid-state emission spectra of complexes **1** (a) and **3** (b) under 370 nm excitation. (c) and (d) Emission spectra at selected temperatures of **1** and **3**, respectively.

Since the large overlap between the ligand band with the Er^{III} transitions, mainly for **1**, a deconvolution of all experimental spectra was performed and the thermometric parameters were calculated (see Table S1 and Fig. S4†). The obtained values are similar to those in Table 1.

To the best of our knowledge, no similar works related to the optical thermometry of Er^{III} complexes have been reported in the literature, in order to perform a direct comparison. However, the optimal values for **1** and **3** are comparable to those of some Er^{III} doped glasses, such as Er^{III}: fluorotellurite,[29] S_r = 0.35% K^{-1}, Er^{III}: oxyfluoride,[30] S_r = 0.41% K^{-1}, and Er^{III}: PbO-Ga_2O_3-SiO_2,[11] S_r = 0.24% K^{-1}.

Color coordinates (CIE) and color correlated temperature (CCT)

The Commission International d'Eclairage (CIE)[31] chromaticity coordinates and CCT values for **1** and **3** were studied as a function of temperature, and are shown in Fig. 6a and b and summarized in Table 2. The differences in CIE 1931 and CCT values for these complexes can be attributed to the thermal dependence of the intraligand and Er^{III} emission bands. The color coordinates for both complexes show a slight shift from (0.209, 0.250 for **1**) and (0.215, 0.303 for **3**) at 17 K, towards (0.200, 0.229 for **1**) and (0.208, 0.290 for **3**) at 300 K. For **1**, the color coordinates are closer to the blue region than for **3**, due to the greater contribution of the intraligand band in the entire temperature range (see Fig. 4a and b).

The thermal dependence of the CCT values (Fig. 6b) for **1** shows an increase from 34 955 K at 17 K to a maximum of 93 909 K at 250 K; the same temperature where the $I_{^4S_{3/2}}/I_{ligand}$ ratio reaches its lower value. Then this value decreases to 72 976 K at 300 K. On the other hand, the CCT values for **3** decrease slightly from 16 173 K at 17 K to 15 720 K at 50 K, and later increase with temperature to 19 330 K at 300 K. As for the CIE coordinates, differences between the CCT values for both complexes can be attributed to the contribution of the ligand emission band, which is greater for **1** than for **3** over all the temperature range.

The CIE coordinates and CCT values obtained for **3** indicate that this complex can be a good candidate for artwork illumination, where the observers prefer a more bluish-white light for painting appreciation than that normally used in museums,[32] or in the well-being, functioning and work performance of office workers.[33]

Metal-centred excitation

Besides the above-mentioned ligand-centred excitation that allows bluish-green and green emissions in the studied complexes, multiple luminescence for **1**, **2** and **3** was observed when metal-centred excitation was used. In all cases, laser excitation at 980 nm produces three up-converted emission bands in the visible range, centred at 523 nm (19 120 cm^{-1}), 542 nm (18 540 cm^{-1}), and 656 nm (15 244 cm^{-1}), which correspond to the bluish-green ($^2H_{11/2}\rightarrow{}^4I_{15/2}$), green ($^4S_{3/2}\rightarrow{}^4I_{15/2}$), and red ($^4F_{9/2}\rightarrow{}^4I_{15/2}$) emission bands of Er^{III} ion, respectively

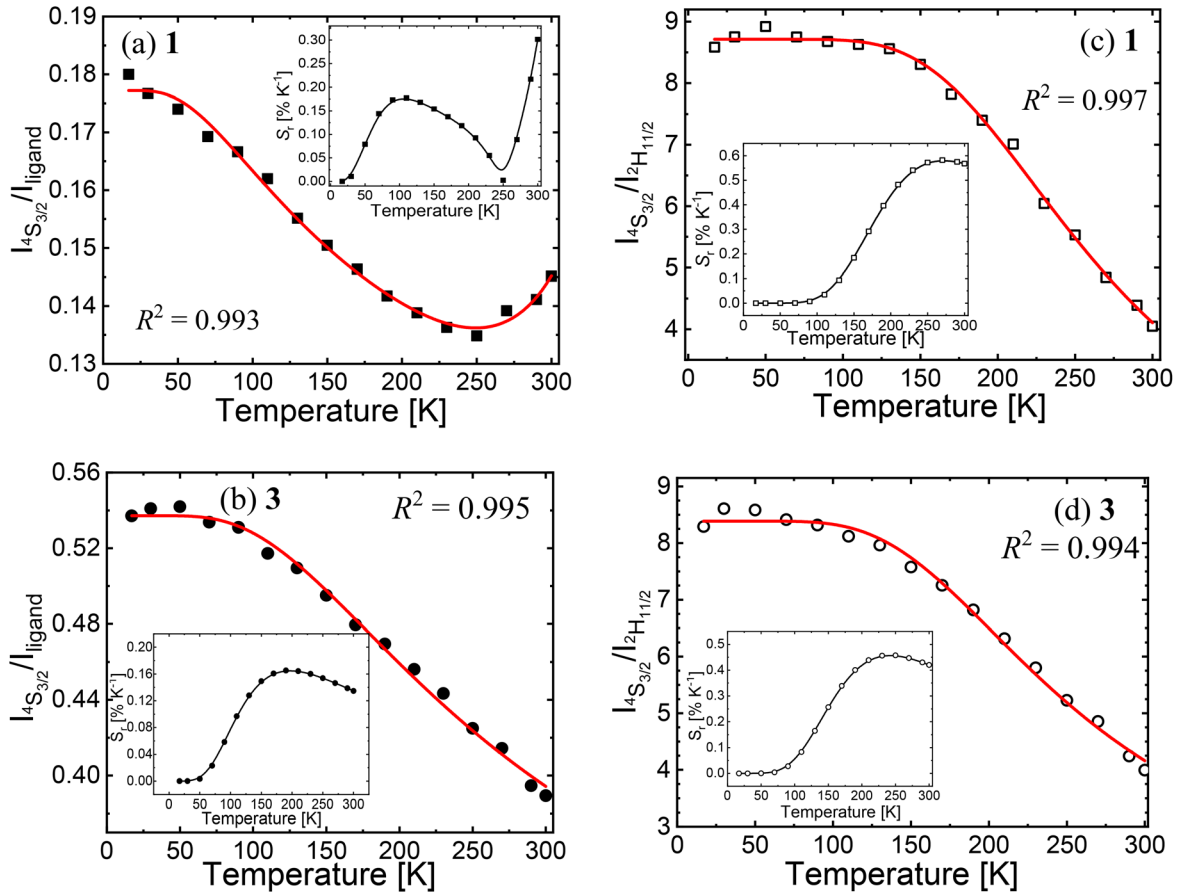

Fig. 5 (a) and (b) Thermal dependence between the integrated areas $I_{^4S_{3/2}}/I_{ligand}$ for **1** and **3**. (c) and (d) Thermal dependence of $I_{^4S_{3/2}}/I_{^2H_{11/2}}$ for **1** and **3**. The points are the experimental data and the red solid lines represent the best fit from eqn (1) and (2), as explained in the experimental section. The insets are the relative sensitivity S_r for **1** and **3**, where the solid lines are guides to the eye.

Table 1 Thermometric parameters ΔE_A and Sr for **1** and **3**

	$I_{^4S_{3/2}}/I_{ligand}$			$I_{^4S_{3/2}}/I_{^2H_{11/2}}$		
Complex	ΔE_A (cm^{-1})	S_r (% K^{-1}) (max)	S_r (% K^{-1}) (300 K)	ΔE_A (cm^{-1})	S_r (% K^{-1}) max	S_r (% K^{-1}) (300 K)
1	157[b] 1769[b]	0.30 (300 K)	0.30	670[a]	0.58 (270 K)	0.57
3	316[a]	0.16 (190 K)	0.13	520[a]	0.46 (250 K)	0.42

[a] ΔE_A: fit with eqn (1). [b] ΔE_A: fit with eqn (2).

(Fig. 7a). Fig. S5† shows the up-conversion spectra of **1**, **2** and **3** samples as a function of pump laser power.

According to Auzel,[16] the up-converted intensity (I_{up}) is proportional to the incident laser pump-power (P) and can be expressed as $I_{up} \propto P^n$. The value of the exponent n represents the number of photons involved in the up-conversion process. Considering the logarithmic form for this equation as follows:

$$\log(I_{up}) = n \log(P) + \text{constant}.$$

The value of n is equal to the slope of a plot of $\log(I_{up})$ *vs.* $\log(P)$. Fig. 7b–d show the $\log(I_{up}) - \log(P)$ plots for the $^2H_{11/2} \rightarrow {}^4I_{15/2}$ (bluish-green), $^4S_{3/2} \rightarrow {}^4I_{15/2}$ (green), and $^4F_{9/2} \rightarrow {}^4I_{15/2}$ (red) transitions of the Er^{III} ion for **1–3**, and reveal a linear dependence with slopes (n) of 1.94, 1.95 and 1.85 (**1**), 2.21, 2.38 and 2.37 (**2**), and 3.17, 3.11 and 2.82 (**3**), respectively. In this way, the up-converted bluish-green, green and red emissions can be explained through the well-known two (for **1** and **2**) and three (for **3**) photon absorption processes.[16,17]

Fig. 8 shows the proposed mechanisms for the up-conversion emission pathways. For the bluish-green and green up-converted emissions in **1** and **2** (Fig. 8-left), it is possible to propose that first the Er^{III} ions are excited from the $^4I_{15/2}$ ground state to the excited $^4I_{11/2}$ level by absorbing one photon

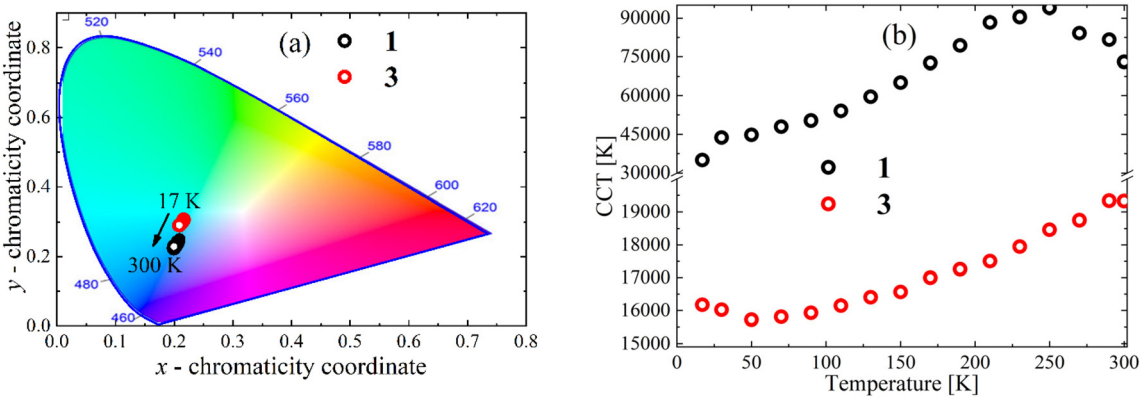

Fig. 6 (a) Positions of CIE 1931 coordinates and (b) CCT values for **1** and **3** as a function of temperature.

Table 2 CIE (*x*, *y*) coordinates and CCT (K) values for complexes **1** and **3** at selected temperatures (λ_{exc} = 370 nm)

Complex	*T* (K)	CIE (*x*, *y*)	CCT (K)
1	17	(0.209, 0.250)	34 955
	50	(0.206, 0.241)	44 782
	150	(0.203, 0.231)	65 106
	250	(0.199, 0.223)	93 909
	300	(0.200, 0.229)	72 976
3	17	(0.215, 0.303)	16 173
	50	(0.216, 0.306)	15 720
	150	(0.215, 0.301)	16 565
	250	(0.210, 0.293)	18 464
	300	(0.208, 0.290)	19 330

with an energy of 980 nm. Even though the lifetime of the $^4I_{11/2}$ level has been reported in the nanosecond range for Er-quinolinolato species,[34] Piguet *et al.*[5,16,17] state that for ErN_9 complexes, the direct excitation to populate the $^4I_{11/2}$ level is not followed by an efficient non-radiative relaxation process to feed the $^4I_{13/2}$ level, instead, a second photon is absorbed. The authors pointed out that the energy splitting of $^4I_{11/2}$ and $^4I_{13/2}$ states is small enough so that no vibrational phonons are available to fill the exact energy gap between these states. Since the splitting of *J* manifolds in Er^{III} ions is associated with the crystal field effect,[5] for **1** and **2**, which also have an ErN_9 coordination, it is feasible that the $^4I_{11/2} \rightarrow {}^4I_{13/2}$ relaxation is sufficiently slowed down to allow for a two-photon absorption process. In this way, a second 980 nm photon is absorbed, promoting the Er^{III} ions to the higher $^4F_{7/2}$ excited state. This process is followed by a non-radiative relaxation to the lower next level, $^2H_{11/2}$, where the emission from the $^2H_{11/2}$ excited state to the $^4I_{15/2}$ ground state gives rise to a bluish-green emission at 522 nm. Moreover, a second non-radiative relaxation from $^2H_{11/2}$ populates the $^4S_{3/2}$ level, and from this excited state, a green emission at 539 nm ($^4S_{3/2} \rightarrow {}^4I_{15/2}$) is obtained.

Besides, for the red up-converted emission in **1** and **2** (*via* two-photon absorption), a third non-radiative process from the $^4S_{3/2}$ to $^4F_{9/2}$ level may produce a red emission at 656 nm, corresponding to the $^4F_{9/2} \rightarrow {}^4I_{15/2}$ transition. This red emission may be obtained through a second mechanism that also involves a two-photon absorption process[27,35] (Fig. 8-left). First, a 980 nm excitation populates the $^4I_{11/2}$ level, followed by a non-radiative relaxation process from the $^4I_{11/2}$ to $^4I_{13/2}$ state. Then, a second photon of 980 nm is absorbed, promoting the $^4I_{13/2}$ level to $^4F_{9/2}$. Finally, the $^4F_{9/2}$ excited level generates the red emission of $^4F_{9/2} \rightarrow {}^4I_{15/2}$. As shown in the next section and in Fig. 8, a downshifted near-infrared Er^{III} emission ($^4I_{13/2} \rightarrow {}^4I_{15/2}$) in **1–3** is obtained through a one-photon absorption process, which indicates that the non-radiative relaxation from $^4I_{11/2}$ to $^4I_{13/2}$ occurs. Furthermore, the contribution of the above described upconversion mechanisms can also be evaluated from the photoluminescence spectra upon ligand-mediated excitation. The indirect excitation (λ_{exc} = 370 nm) allows the population of the $^2H_{11/2}$ and $^4S_{3/2}$ levels, with which bluish-green and green emission bands were detected (Fig. 2). However, the red emission ($^4F_{9/2} \rightarrow {}^4I_{15/2}$) was not observed, indicating that the non-radiative process from $^4S_{3/2}$ to $^4F_{9/2}$ level lacks efficiency. This behaviour is in agreement with some reported Er^{III}-doped inorganic hosts.[10,34,35] Therefore, we can conclude that the first mechanism will not contribute to the red up-conversion in **1** and **2**, with the second mechanism being the feasible pathway.

For **3**, the mechanism proposed for bluish-green and green up-converted emissions *via* a three-photon absorption process (Fig. 8-right) comprises first the population of the $^4F_{7/2}$ excited state by means of the process described previously (by two-photon absorption), followed by multiple non-radiative relaxations to the $^4I_{9/2}$ level, where a third photon is absorbed to reach the $^4F_{3/2}$ level. Then, a second multiple non-radiative decay populates the thermally coupled emitting states, $^2H_{11/2}$ and $^4S_{3/2}$, from which the bluish-green ($^2H_{11/2} \rightarrow {}^4I_{15/2}$) and green ($^4S_{3/2} \rightarrow {}^4I_{15/2}$) emission bands are generated. For the red up-converted emission in **3**, the proposed three-photon absorption mechanism also occurs through the initial population of the $^4F_{7/2}$ excited state. Then, multiple non-radiative relaxations populate the $^4I_{13/2}$ level, where a third photon is absorbed, reaching the $^4F_{9/2}$ excited state and generating the

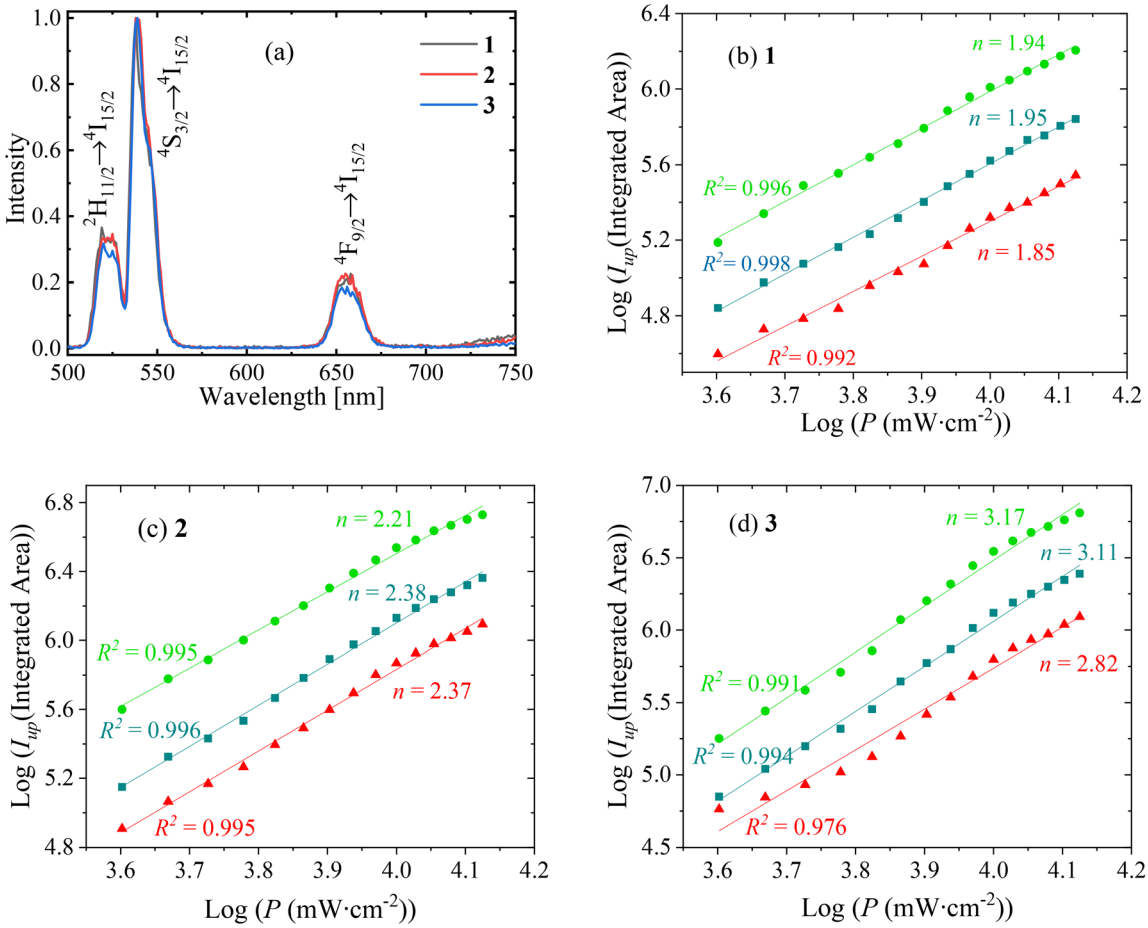

Fig. 7 (a) Normalized up-conversion emission spectra of complexes **1–3** at room temperature under 980 nm laser excitation with a power of 1900 mW. Log–log plots of the up-converted intensities for the $^2H_{11/2} \rightarrow {}^4I_{15/2}$ (bluish-green), $^4S_{3/2} \rightarrow {}^4I_{15/2}$ (green) and $^4F_{9/2} \rightarrow {}^4I_{15/2}$ (red) transitions (I_{up}) as a function of incident pump intensities (P, in mW cm^{-2}) focused on a spot size of 0.15 cm^2 for **1** (b), **2** (c) and **3** (d). The straight lines correspond to linear fits.

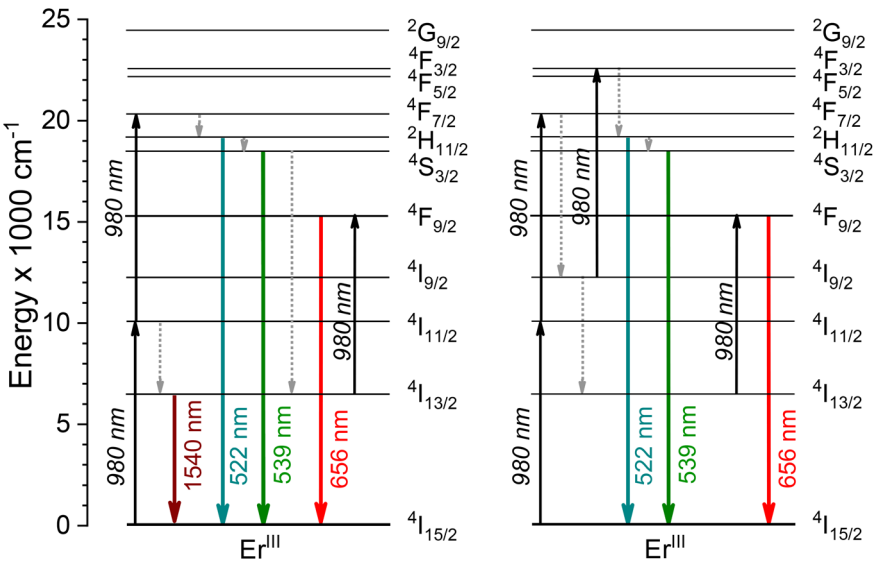

Fig. 8 Er^{III} centred energy levels showing possible up-conversion pathways *via* two- (left) and three-photon (right) absorption, and downshifting *via* one-photon absorption (left) under 980 nm laser excitation.

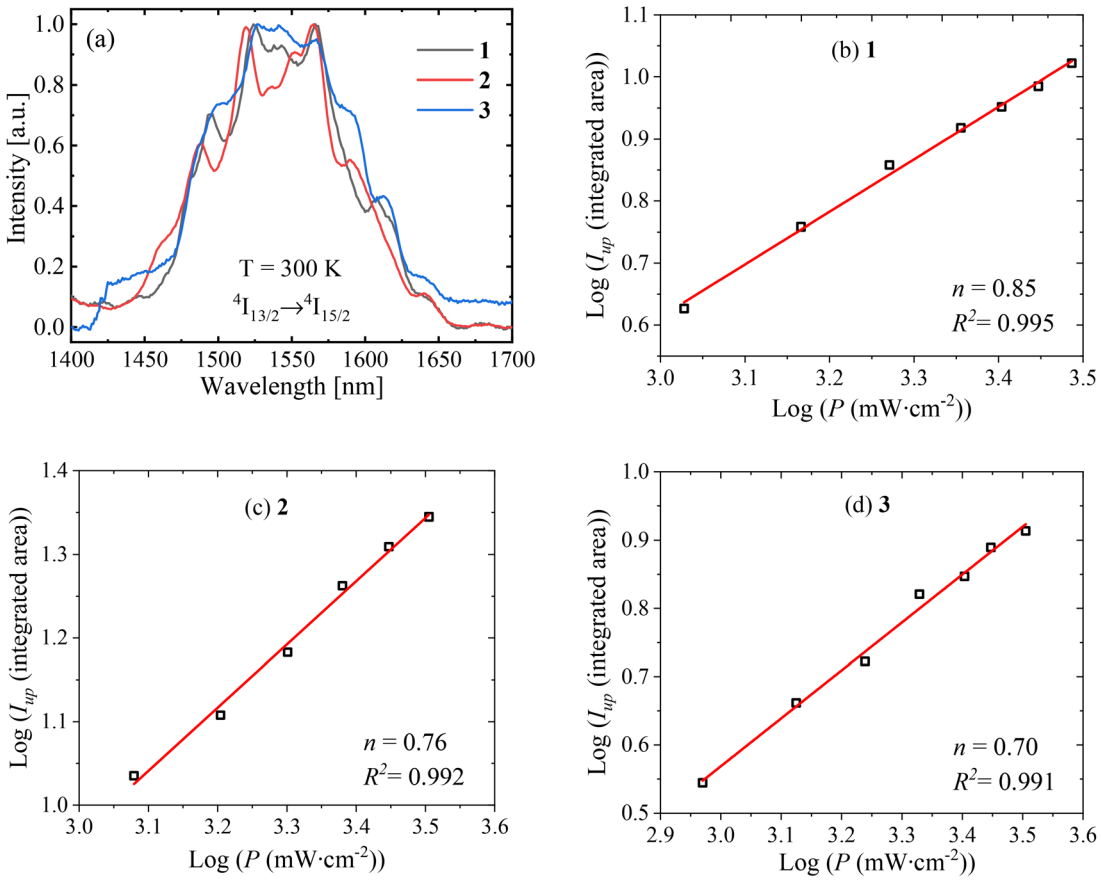

Fig. 9 (a) Near-infrared downshifted Er($^4I_{13/2} \rightarrow {}^4I_{15/2}$) emission observed for complexes **1–3** at room temperature under 980 nm laser excitation with a power of 240 mW. Log–log plots of downshifted intensities (I_{up}) as a function of incident pump intensities (P, in mW cm^{-2}) focused on a spot size of 0.075 cm^2 for **1** (b), **2** (c), and **3** (d). The straight red lines correspond to linear fits.

red emission of $^4F_{9/2} \rightarrow {}^4I_{15/2}$ (Fig. 8-right). This three-photon absorption process is in agreement with the mechanisms described by Piguet *et al.*[5]

Interestingly, red up-conversion has not been detected in several reported molecular complexes based on Er^{III}, in contrast to the bluish-green and green emissions, which are reported.[5,15–17,36] To the best of our knowledge, the Er^{III} complexes **1–3** are the first mononuclear species with a known crystal structure, where erbium-centred excitation produces red up-conversion emission in the solid state, together with the bluish-green and green bands.[37]

Moreover, upon excitation with a 980 nm laser a weak emission in the NIR region was also observed. Fig. 9 shows the normalized solid-state near infrared emission spectra of **1**, **2** and **3** taken at room temperature. In all cases, a broad band between 1440 and 1650 nm was detected, corresponding to the $^4I_{13/2} \rightarrow {}^4I_{15/2}$ transition of the Er^{III} ion (Fig. 9a). Fig. S6† show the infrared spectra of **1**, **2** and **3** as a function of the laser power.

The slopes (n) of the corresponding log(I_{up}) *vs.* log(P) plots were estimated as 0.85 (**1**), 0.76 (**2**) and 0.70 (**3**) (Fig. 9b–d). These values are compatible with a mechanism through one-photon absorption (Fig. 8-left), which involves the direct excitation of the Er^{III} ion with 980 nm radiation to populate the $^4I_{11/2}$ excited level at *ca.* 10 100 cm^{-1}. Then, a non-radiative relaxation from the $^4I_{11/2}$ to $^4I_{13/2}$ level occurs to give rise to the near-infrared downshifted Er($^4I_{13/2} \rightarrow {}^4I_{15/2}$) emission.[38,39] It is notable that the emission bands of all three complexes present large full width at half-maximum values (*ca.* 109, 116, and 114 nm) for **1**, **2**, and **3** respectively, which can enable the use of these complexes as optical amplifiers in telecommunications devices operating at 1540 nm.[40]

Conclusions

The optical properties of three Er^{III} hexaazamacrocyclic complexes were studied. Complexes with aliphatic spacers (**1** and **3**) on the macrocyclic ligand show, under excitation at 370 nm, bluish-green and green emission bands, while the one with the aromatic spacer (**2**) only presents ligand emission, evidencing a structural dependence of the energy transfer from the ligand to the Er^{III} emission levels. The thermal emission behaviour of complexes **1** and **3** indicates that these materials exhibit a good optical thermometric parameter S_r, 0.58% K^{-1} (270 K) for **1** and 0.46% K^{-1} (250 K) for **3**, conferring them the possibility of being used as thermosensors. For **1** and **3**, the

CIE coordinates are shifted to the bluish-green region due to the contribution of the ligand emission, and show a slight temperature dependence. In addition, **1** and **3** present a faint NIR emission at *ca.* 1500 nm. On the other hand, erbium-centred excitation with 980 nm light allows the observation of bluish-green, green and red up-conversion emissions, as well as downshifted NIR emission at *ca.* 1500 nm. For this last emission, a mechanism involving one-photon absorption is evidenced in all cases. On the other hand, up-converted emission bands can be described by two (**1** and **2**) and three (**3**) photon absorption mechanisms. In summary, we demonstrated that the use of hexaazamacrocyclic ligands is a suitable strategy for obtaining molecular dual Er^{III}-centred visible/NIR emitters, which can be tuned by chemical design, leaving room to explore new luminescent erbium(III) molecular complexes.

Author contributions

Conceptualization: YG, RCS, and ES; data curation: RCS, YG, and PF; formal analysis: RCS, YG, JM, and ES; investigation and methodology: YG, RCS, PFC, and LGM; writing – original draft: YG; and writing – review and editing: YG, RCS, PF, LGM, ASSC, and ES.

Conflicts of interest

The authors declare no competing financial interest.

Acknowledgements

YG, JM and ES acknowledge the financial support from the FONDECYT 1200033 grant. YG thanks the National Agency for Research and Development (ANID) for the Doctoral Scholarship 21170520 and the FONDECYT Postdoctoral Project 3220200. PF and PFC thank ANID for Proyecto de Iniciación 11200919. This study was financed in part by the Brazilian agencies, Conselho Nacional de Desenvolvimento Científico e Tecnológico (CNPq), Fundação de Amparo à Pesquisa do Estado de Goiás (FAPEG) and Financiadora de Estudos e Projetos (FINEP). RCS thanks the CNPq research fellowship 310307/2021-0. ASSC and LGM acknowledge Fundação de Amparo à Pesquisa do Estado de São Paulo (FAPESP) for the grants 2013/07793-6 (CeRTEV – Center for Research, Technology and Education in Vitreous Materials) and 2019/21770-5 (postdoctoral fellowship).

References

1 R. Marin, G. Brunet and M. Murugesu, Shining New Light on Multifunctional Lanthanide Single-Molecule Magnets, *Angew. Chem., Int. Ed.*, 2021, **60**, 1728–1746.
2 D. Parker, J. D. Fradgley and K.-L. Wong, The Design of Responsive Luminescent Lanthanide Probes and Sensors, *Chem. Soc. Rev.*, 2021, **50**, 8193–8213.
3 J.-C. G. Bünzli and S. V. Eliseeva, Lanthanide NIR Luminescence for Telecommunications, Bioanalyses and Solar Energy Conversion, *J. Rare Earths*, 2010, **28**, 824–842.
4 J.-C. G. Bünzli, Lanthanide Luminescence for Biomedical Analyses and Imaging, *Chem. Rev.*, 2010, **110**, 2729–2755.
5 B. Golesorkhi, H. Nozary, A. Fu and C. Piguet, Erbium Complexes as Pioneers for Implementing Linear Light-Upconversion in Molecules, *Mater. Horiz.*, 2020, **7**, 1279–1296.
6 A. Nadort, J. Zhao and E. M. Goldys, Lanthanide Upconversion Luminescence at the Nanoscale: Fundamentals and Optical Properties, *Nanoscale*, 2016, **8**, 13099–13130.
7 K. L. Wong, J.-C. G. Bünzli and P. A. Tanner, Quantum Yield and Brightness, *J. Lumin.*, 2020, **224**, 117256.
8 H. Bolvin, A. Fürstenberg, B. Golesorkhi, H. Nozary, I. Taarit and C. Piguet, Metal-Based Linear Light Upconversion Implemented in Molecular Complexes: Challenges and Perspectives, *Acc. Chem. Res.*, 2022, **55**, 442–456.
9 F. Auzel, Upconversion and Anti-Stokes Processes with f and d Ions in Solids, *Chem. Rev.*, 2004, **104**, 139–174.
10 T. Jung, H. L. Jo, S. H. Nam, B. Yoo, Y. Cho, J. Kim, H. M. Kim, T. Hyeon, Y. D. Suh, H. Lee and K. T. Leed, The Preferred Upconversion Pathway for the Red Emission of Lanthanide-Doped Upconverting Nanoparticles, NaYF4: Yb^{3+}, Er^{3+}, *Phys. Chem. Chem. Phys.*, 2015, **17**, 13201–13205.
11 W. A. Pisarski, J. Pisarska, R. Lisiecki and W. Ryba-Romanowski, Sensitive Optical Temperature Sensor Based on Up-Conversion Luminescence Spectra of Er^{3+} Ions in $PbO–Ga_2O_3–XO_2$ (X=Ge, Si) Glasses, *Opt. Mater.*, 2016, **59**, 87–90.
12 P. S. Zangabad, M. Karimi and F. Mehdizadeh, Nanocaged Platforms: Modification, Drug Delivery and Nanotoxicity, *Nanoscale*, 2017, **9**, 1356–1392.
13 A. Beeby, I. M. Clarkson, R. S. Dickins, S. Faulkner, D. Parker, L. Royle, A. S. De Sousa, J. A. G. Williams and M. Woods, Non-Radiative Deactivation of the Excited States of Europium, Terbium and Ytterbium Complexes by Proximate Energy-Matched OH, NH and CH Oscillators: An Improved Luminescence Method for Establishing Solution Hydration States, *J. Chem. Soc., Perkin Trans. 2*, 1999, **2**, 493–503.
14 W. S. Lo, W. T. Wong and G. L. Law, Friend or Foe? The Role of Solvents in Non-Triplet, Intraligand Charge Transfer Sensitization of Lanthanide(III) Luminescence, *RSC Adv.*, 2016, **6**, 74100–74109.
15 B. Golesorkhi, H. Bolvin and C. Piguet, Molecular Light-Upconversion: We Have Had a Problem! When Excited State Absorption (ESA) Overcomes Energy Transfer Upconversion (ETU) in Cr(III)/Er(III) Complexes, *Dalton Trans.*, 2021, **50**, 7857–8260.
16 B. Golesorkhi, A. Fürstenberg, H. Nozary and C. Piguet, Deciphering and Quantifying Linear Light Upconversion in

Molecular Erbium Complexes, *Chem. Sci.*, 2019, **9**, 6876–6885.

17 B. Golesorkhi, H. Nozary, L. Guénée, A. Fürstenberg and C. Piguet, Room-Temperature Linear Light Upconversion in a Mononuclear Erbium Molecular Complex, *Angew. Chem., Int. Ed.*, 2018, **57**, 15172–15176.

18 B. Golesorkhi, L. Guénée, H. Nozary, A. Ferstenberg, Y. Suffren, S. V. Eliseeva, S. Petoud, A. Hauser and C. Piguet, Thermodynamic Programming of Erbium(III) Coordination Complexes for Dual Visible/Near-Infrared Luminescence, *Chem. – Eur. J.*, 2018, **25**, 13158–13169.

19 Y. Gil, P. Fuentealba, A. Vega, E. Spodine and D. Aravena, Control of Magnetic Anisotropy by Macrocyclic Ligand Distortion in a Family of Dy^{III} and Er^{III} Single Molecule Magnets, *Dalton Trans.*, 2020, **49**, 17709–17718.

20 P. Fuentealba, D. Villagra, Y. Gil, H. Aguilar-Bolados, P. R. C. de Santana, G. Gasparotto, A. Vega, J. Manzur and E. Spodine, Thermal Dependence of the Luminescent Properties of Mononuclear Tb^{III} Macrocyclic Complexes, *Eur. J. Inorg. Chem.*, 2021, **25**, 4543–4551.

21 D. Mara, F. Artizzu, B. Laforce, L. Vincze, K. Van Hecke, R. Van Deun and A. M. Kaczmarek, Novel Tetrakis Lanthanide β-Diketonate Complexes: Structural Study, Luminescence Properties and Temperature Sensing, *J. Lumin.*, 2019, **213**, 343–355.

22 G. H. Dieke, *Spectra and Energy Levels of Rare Earth Ions in Crystals*, Wiley-Interscience, New York, USA, 1968.

23 S. I. Weissman, Intramolecular Energy Transfer The Fluorescence of Complexes of Europium, *J. Chem. Phys.*, 1942, **10**, 214–217.

24 T. Som and B. Karmakar, Efficient Green and Red Fluorescence Upconversion in Erbium Doped New Low Phonon Antimony Glasses, *Opt. Mater.*, 2009, **31**, 609–618.

25 D. K. Sardar, S. Chandrasekharan, K. L. Nash and J. B. Gruber, Optical Intensity Analyses of Er^{3+}:$YAlO_3$, *J. Appl. Phys.*, 2008, **104**, 023102.

26 Y. Cui, H. Xu, Y. Yue, Z. Guo, J. Yu, Z. Chen, J. Gao, Y. Yang, G. Qian and B. Chen, A Luminescent Mixed-Lanthanide Metal–Organic Framework Thermometer, *J. Am. Chem. Soc.*, 2012, **134**, 3979–3982.

27 V. Klinkov, V. Aseev, A. Semencha and E. Tsimerman, Temperature Sensor Based on Upconversion Luminescence of Er^{3+}-Doped Fluoroaluminate Glasses, *Sens. Actuators, A*, 2018, **277**, 157–162.

28 X. Wang, Q. Liu, Y. Bu, C.-S. Liu, T. Liua and X. Yan, Optical Temperature Sensing of Rare-Earth Ion Doped Phosphors, *RSC Adv.*, 2015, **5**, 86219–86236.

29 S. F. León-Luis, U. R. Rodríguez-Mendoza, E. Lalla and V. Lavín, Temperature Sensor Based on the Er^{3+} Green Upconverted Emission in a Fluorotellurite Glass, *Sens. Actuators, B*, 2011, **158**, 208–213.

30 L. Feng, B. Lai, J. Wang, G. Du and Q. Su, Spectroscopic Properties of Er^{3+} in a Oxyfluoride Glass and Upconversion and Temperature Sensor Behaviour of Er^{3+}/Yb^{3+}-Codoped Oxyfluoride Glass, *J. Lumin.*, 2010, **130**, 2418–2423.

31 C. Wyman, P.-P. Sloan and P. Shirley, Simple Analytic Approximations to the CIE XYZ Color Matching Functions, *J. Comput. Graph. Tech.*, 2013, **2**, 1–11.

32 P. D. Pinto, J. M. M. Linhares and S. M. C. Nascimento, Correlated Color Temperature Preferred by Observers for Illumination of Artistic Paintings, *J. Opt. Soc. Am. A*, 2008, **25**, 623.

33 P. R. Mills, S. C. Tomkins and L. J. Schlangen, The Effect of High Correlated Colour Temperature Office Lighting on Employee Wellbeing and Work Performance, *J. Circadian Rhythms*, 2007, **5**, 2.

34 F. Artizzu, F. Quochi, L. Marchio, E. Sessini, M. Saba, A. Serpe, A. Mura, M. L. Mercuri, G. Bongiovanni and P. Deplano, Fully Efficient Direct Yb-to-Er Energy Transfer at Molecular Level in a Near-Infrared Emitting Heterometallic Trinuclear Quinolinolato Complex, *J. Phys. Chem. Lett.*, 2013, **4**, 3062–3066.

35 X. Zhang, B. Li, L. Zhang and H. Zhao, Metal-Organic Frameworks Modulated by Doping Er^{3+} for Up-conversion Luminescence, *Appl. Mater. Interfaces*, 2016, **8**, 17389–17394.

36 B. Golesorkhi, S. Naseri, L. Guenee, I. Taarit, F. Alves, H. Nozary and C. Piguet, Ligand-Sensitized Near-Infrared to Visible Linear Light Upconversion in a Discrete Molecular Erbium Complex, *J. Am. Chem. Soc.*, 2021, **143**, 15326–15334.

37 G. Sun, Y. Ren, Y. Song, Y. Xie, H. Zhang and L. Sun, Achieving Photon Upconversion in Mononuclear Lanthanide Molecular Complexes at Room Temperature, *J. Phys. Chem. Lett.*, 2022, **13**, 8509–8515.

38 Y. Zhong and H. Dai, A Mini-Review on Rare-Earth down-Conversion Nanoparticles for NIR-II Imaging of Biological Systems, *Nano Res.*, 2020, **13**, 1281–1294.

39 D. Mara, F. Artizzu, P. F. Smet, A. M. Kaczmarek, K. Van Hecke and R. Van Deun, Vibrational Quenching in Near-Infrared Emitting Lanthanide Complexes: A Quantitative Experimental Study and Novel Insights, *Chem. – Eur. J.*, 2019, **25**, 15944–15956.

40 X. Guo, H. Guo, L. Fu, L. D. Carlos, R. A. S. Ferreira, L. Sun, R. Deng and H. Zhang, Novel Near-Infrared Luminescent Hybrid Materials Covalently Linking with Lanthanide [Nd(III), Er(III), Yb(III), and Sm(III)] Complexes via a Primary β-Diketone Ligand: Synthesis and Photophysical Studies, *J. Phys. Chem. C*, 2009, **113**, 12538–12545.